Egyptian Journal of Chemistry

http://ejchem.journals.ekb.eg/

Impact of Welding Processing Parameters on The Microstructure Grain Refinement and Hardness Behavior of The Aluminum AA1050

Ahmed Saad Hassan, Essam B. Moustafa*, S. S. Mohamed

Mechanical Engineering Department, Shoubra Faculty of Engineering, Benha University, Cairo, Egypt

Abstract

In the current Investigation, AA1050 aluminum rolled sheets were welded using the friction stir welding technique (FSW). The effect of the processing parameters on the welding quality and grain refinement is discussed; hence, four rotation and traverse speeds are used to evaluate the welding characteristics. The heat generated during welding significantly affects the resultant welded joint, mechanical properties, and materials quality. The microstructure examination using polarized optical microscopy was employed to inspect the grain size and refinement during welding. The microstructure analysis revealed that ultra-fine grains were formed for all investigated samples, but the lower rotational speed significantly improved the grains' reduction by about 63.4% compared to the base alloy. In contrast, the welded stirred zone reduced the microhardness with respect to the base metal by about 24.5 % due to the higher heat generated between the FSW tool and the base welded sheets. The metal transfer rate did not alter FSW weld hardness values in this investigation. The current research also shows that a faster metal transfer rate reduces weld porosity, which lowers FSW weld hardness.

Keywords: FSW; AA1050; Microstructure; Microhardness; Grain; Refinement.

1. Introduction

Friction stir welding (FSW) is a modern joining process developed and patented by the British Welding Institute (TWI)[1]. Because the procedure is new, specialized equipment known as "friction stir welders" is not yet frequently utilized in practice and is rather costly. Various aluminum alloys ranging in strength from high to moderate have been machined using FSW and adapted milling machines [2-4]. Due to the higher temperature and the extensive plastic deformation caused by the stirring action of the tool pin, the grain structure inside the nugget is fine and equiaxed, and the grain size is much smaller than that of the base material. In friction stir welding (FSW), the tool is used as a stirrer to extrude the material in the welding direction. Recrystallization and dynamic recovery rates are extremely sensitive to deformation temperature and strain rate [5-7]. The microstructure of the nugget was made up of grains that had recrystallized and shrunk in size by an average of 10 times. The combined action of heat and deformation caused microstructural alterations in TMAZ. This resulted in grain boundary embrittlement and a consequent reduction in the strength of the GMA weld joint [8]. The nugget's microstructure at the welded junction of AA2219 alloy was made up of recrystallized grain structure with a 10-fold decrease in average grain size. The impacts of heat and deformation on TMAZ caused changes in its microstructure [9]. The welding zone undergoes dynamic recrystallization due to the high deformation and moderate temperature, resulting in a modified microstructure with a grain size ranging from 2 to 10 micrometers.

After undergoing the FSW procedure, the welding zone looks like a ring structure, somewhat unlike onion rings [10, 11]. Because of how quickly the welding zone cools, only stable phases may develop there, and the formation of any new phases is prevented. It's also worth noting that, owing to the random crystallization of sediments on dislocations, the crystallization process shifts from a homogeneous to a non-homogeneous condition in this area [12-14]. The rolled plates of AA 6061 aluminum alloy were joined. There were refined, equiaxed grains and uniformly dispersed, highly fine-strengthening precipitates in the weld zone, giving FSW joints exceptional tensile strength. Due to its hardness and finer microstructure, the FSW-made joint beat the control joint in tensile and notched impact strength [15]. While the yield strength of TIG welded Al-Mg-Sc alloys is similar to that of the base metal, friction stir welded joints to have a 20% lower yield strength, according to [16]. In addition, several investigations

*Corresponding author e-mail: essbahgat@gmail.com; (Essam B. Mostafa).

Receive Date: 13 January 2023, **Revise Date:** 15 March 2023, **Accept Date:** 22 March 2023,
First Publish Date: 22 March 2023
DOI: 10.21608/EJCHEM.2023.187195.7448

have identified the most critical factors that affect the qualities of friction stir welded joints. They studied how those parameters affect the weld properties, which was a significant focus of the study[17-22]. Tool speed, welding speed, axial force, and other factors of the FSW process affect weld quality. The quality of the base material was compared with the parameters of the FSW process. FSW joints were made with five aluminum alloys (AA 1050, AA 6061, A.A. 2024, AA 7039, and AA 7075) and different process conditions according to[23]. The quality of the welds was evaluated microstructurally (defective or defect-free). The tool speed and the welding speed correlate empirically with the properties of the base metal. The impact of process parameters such as tool shoulder diameter, tool pin design, tool speed, and welding speed has been investigated on the mechanical and metallurgical characteristics of the aerospace aluminum alloy 5052 [24]. The development of an analytical model to estimate the weld's thermal profile is investigated [25]. The thermal gradients generated during the welding process can be predicted and used to optimize the tool's design. The prediction model was developed based on [26]. The experimental results of the study showed that the variation in friction heat generation rate from the pin varies considerably depending on the tool geometry and the welding parameters used.

Therefore, the importance of studying the effect of process parameters of the FSW process on the microstructure refinement of the welded zone has a major impact on the quality of the weld. The relationship between the processing parameters (welding speed and tool speed) and the welded zone's quality is evident in the nugget zone's microstructure, hardness, and heat generation. Therefore, many authors focus only on the effects of the welding process parameters on the mechanical and microstructural properties without considering the correlation between the studied properties. In the current Investigation, AA1050 wrought alloy is used in the welding process as the base metal; hence, the automatic milling machine is utilized to perform the FSW process.

2. Experimental Procedure

2.1 Materials and Methods

In this study, AA 1050 wrought plates with the elemental composition (Table 1) were used, and their compositions were validated by inductively coupled plasma optical emission spectroscopy. A wire-cutting machine was used to cut samples with 150 mm x 50 mm x 8 mm dimensions. An automatic vertical milling machine was used for friction stir welding. A specially designed and constructed FSW fixture was used for clamping. H10 tool steel was used for the FSW process's cutting tools. Following the machining process, the tool's hardness was increased by hardening it in oil, also known as "quenching." The tool had a pin with a profile that was conical and cylindrical at the same time. Using high-carbon steel, a rotating, non-consumable tool was created and put into use; hence, the designed tool was recommended by [25-27]. The end probe diameter is 5.5 mm, with a 25 mm shoulder diameter and a 6 mm length pin, as shown in Fig. The tilt angle of the tool was maintained at a constant 2 degrees throughout the operation.

Table 1 Chemical composition of Al 1050-0 aluminum alloy (wt. %).

Mn%	Fe %	Cu %	Mg %	Si %	Zn %	Al
0.05	0.41	0.05	0.05	0.26	0.07	Remain

2.2 Microstructure Preparation

Etching was applied to highly polished, welded specimens to expose the microstructure and prepare them for microscopy examination. First, these specimens were polished to the higher polish required for an aluminum alloy of this type (200–2000 emery paper). Then the specimens were ground with a diamond paste to obtain a smooth surface. The black residues formed during lapping were removed with running water and cleaned with cotton after drying. The samples were etched with a solution called Keller's reagent, which consisted of 2 ml hydrofluoric acid, 2 ml hydrochloric acid, and 190 ml water [28]. A microstructural study of the friction stir welded samples was performed to investigate the effects of the process parameters on the grain structure. An optical metallurgical microscope, model GX41, was used to examine the microscopic structures of the FSW specimens.

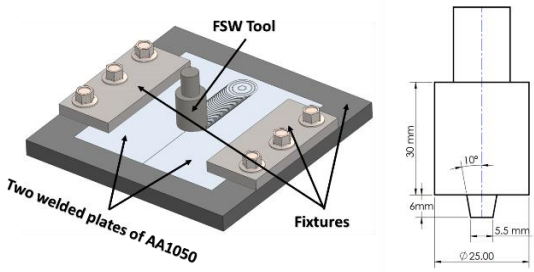

Fig 1 Schematic drawing of the FSW process and the FSW tool design

3. Results and Discussions

3.1 Microstructure Observation

Processing parameters such as tool speed and longitudinal travel speed affect the material's flow behavior. The microstructural behavior was also influenced. By visually inspecting the welds at different rotational and travel speeds, we can see that the rotational speed significantly impacts the weld surface-to-travel speed (ω/v) ratio. A surface weld that is both smooth and defect-free can be achieved by increasing the value of ω/v. A good deal of material can be pushed into the weld area due to the high ω/v

welding heat input. Therefore, welding with high quality and a good weld surface is achieved by altering the speed ratios (ω/v), which can be anywhere from 11 to 32. Different welding parameters were used to study the cross-sections of welded connections. No signs of cracking or porosity were evident, indicating that the joints were of higher quality, as shown in Fig.2a. Heat Affected Zone (HAZ), Thermo-mechanically Affected Zone (TMAZ), and Stirred Zone (S.Z.) are the three zones that emerge during the FSW process, as revealed by [29, 30] and depicted in Fig.2-b.

Extensive softening and plastic deformation of the S.Z. leads to a recrystallized fine-grain structure. The TMAZ is a tiny, distorted-grain region surrounding the WNZ and sees less plastic strain than the rest of the zone. Finally, as shown in Fig. 2-b, the HAZ is the most vulnerable part of the FSW process. The microstructure images of HAZ at different welding parameters show that all stirred zones have finer grains than the heat-affected zones. The microstructure of the heat-affected zones evidences this. This is due to the strong plastic deformation and high temperature, which led to the dynamic recrystallization of the material.

The relationship between the HAZ microstructure and the welding parameters is surprisingly similar to the stirred zone microstructure. Microstructure modifications in the AA1050 alloy were produced using friction stir welding. Optical microscopy showed that the grain structure was severely bowed due to deformation in the TMAZ. However, the dynamic recrystallization (DRX) nugget had significantly smaller grains and was more equiaxed than those seen in the elongated and scone metal matrix. Developing a grain/sub-grain size in the stirred zone during FSW indicates recrystallization via a CDRX process. This was determined by contrasting the grain size formed in FSW with that developed in AA 1050 alloys after rolling processing [31]. The microstructure behavior was also influenced. The average grain size and the aspect ratio are calculated using JMicroVision software.

The average grain intercept (AGI) method is used for the calculations. When a line intersects a grain boundary, the program is applied to create the intercept lines and measure the line length. The following formulas are used to determine the average grain size:

AGI = (number of intercepts) / (line length).

Grain aspect ratio = (AVG grain size in X-direction)/ (AVG grain size in Y-direction).

The microstructure grain size analysis shows that the base alloy's average grain size is approximately 44.6 ±16.2 μm, and the aspect ratio is about 23.5%. Figure 4 shows the optical microstructure image of the AA1050 alloy base metal as a rolled sheet; hence the grains are elongated horizontally with a small thickness observed. It is not unusual for a single quantity measurement to be sufficient to meet the measurement's expectations. However, it is impossible to quantify the uncertainty of a single measurement. In attempting to estimate the uncertainty of a single measurement, the judgment of the experimenter is required. It is incumbent upon the experimenter to estimate the uncertainty of any single measurement, which is limited by the precision and accuracy of the measuring device and any other factors that might affect the experimenter's ability to make the measurement.

The uncertainty analysis was calculated according to each processing parameter in addition to the base metal grain size; hence, there were 10 AGIs values for each condition, as illustrated in Table 2. The subgrain size in these deformation modes has been found to depend on the Zenner-Hollomon parameter $Z = \varepsilon e^{(\frac{Q}{(RT)})}$, where ε and T stand for the strain rate and temperature of the deformation, Q is the activation energy of the process, and R.T. is the strain rate.

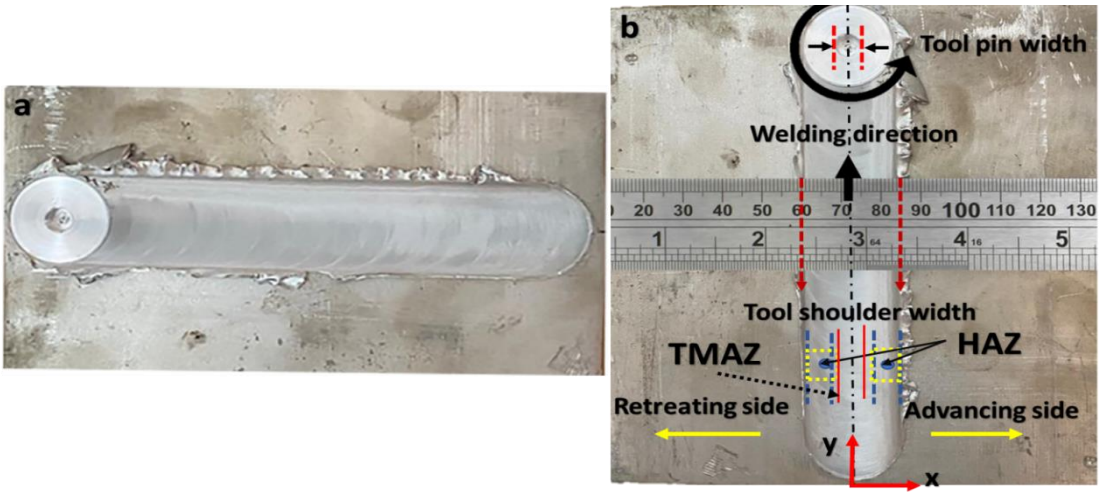

Fig. 2 (a) typical image of the FSW samples with free defect welds, (b) An illustration of the FSW, including the axes; hence The x–y plane is transverse to the direction of tool advance

Table 2 Uncertainty analysis of the grain size according to the welding processing parameters

Too rotation speed (RPM)	Tool travel speed (mm/min)	AVG. Grain size (µm)	Uncertainty (±µm)	Rotation /welding speed ratio (ω/v)	Grain size reduction (%)
450	14	16.32	3.17	32.1	63.4
	20	18.42	2.52	22.5	58.7
	28	19.44	3.88	16.1	56.4
	40	22.15	4.54	64.3	50.3
560	14	26.78	7.43	35.5	39.9
	20	32.02	7.62	17.8	28.2
	28	25.04	8.2	11.3	43.9
	40	23.51	4.75	14	47.3
710	14	26.54	3.03	22.5	40.5
	20	21.66	5.29	20	51.4
	28	25.51	2.49	25.4	42.8
	40	21.78	1.46	32.1	51.2
900	14	20.9	6.63	50.7	53.1
	20	31.31	8.16	40	29.8
	28	26.02	4.14	45	41.7
	40	23.73	5.74	28	46.8
Base alloy	-----	44.6	16.18	----	00

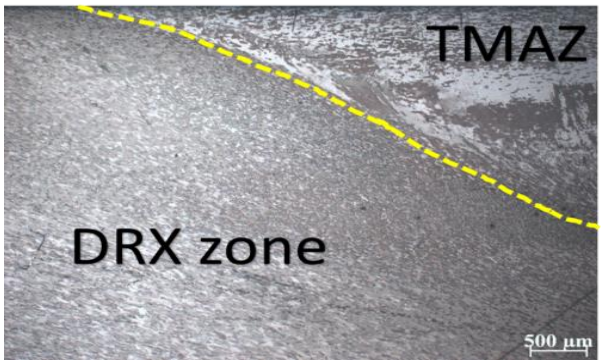

Fig. 3 An optical microscope image of the thermomechanical affected zone (TMAZ) and the dynamically recrystallized zone (DRX) of the AA1050 alloy.

In Fig. 5, we see optical microscope images of the stir zone produced by varying the welding conditions; hence refined and semi-equiaxed grains are observed in microstructures across all FSW conditions. For a given velocity, larger grain sizes are produced in the stir zone as the rotational speed increases. According to the literature-described relationship between heat input and ω/v ratio, the heat input increases with increasing rotational speed. As a result, recrystallization leads to high grain development, and the ω/v ratio increases the heat input and the rotational speed. The higher interface ω/v ratio improves heat transfer into the FSW joint. This leads to poor weld integrity, especially at low ω/high v speed. Fig. 6 shows the effect of different rotational (ω), and retraction (v) speeds on microstructure development in the heat-affected zone of the stirred zone. As the R and W speeds decrease, there is an increase in porosity formation, a decrease in grain size, and finally, the formation of a coarse equiaxed structure, as shown in Fig. 5 c,d.

On the other hand, the heat input is lowest at the high ω/low v speed because the heat transfer from the FSW interface to the base material is low, resulting in poor preheating (Fig.6 a,b). This is attributed to insufficient preheating at lower ω and v speeds, leading to partial melt droplets forming. Since the stirring speed is lower, more melt can be deposited on the base material, forming a coarse equiaxed structure within the heat-affected zone. In addition, the average size of the heat-affected zone increases with decreasing v and ω speeds. There is less agitation at lower agitation speeds, which leads to an increase in the local temperature of the FSW compound as energy is absorbed from the material being melted.

The aspect ratio of the grains in the stirred zone expresses the equiaxed grains generated due to the combination of the tool rotation speed and the traverse speed. Fig. 7 shows that at 710 rpm, the more equiaxed grains are formed with a higher welding travel speed of 28 and 40 mm/min. Figures 8 and 9 show the processing parameters' effect (rotational tool speed and welding speed) on the AVG. When the rotational speed is reduced, the grain size is reduced, resulting in ultra-fine grains generated during the welding process. While increasing the rotational speed, the grain becomes coarser, which can be explained by the insufficient heat generated during the welding process. The lower travel speed causes the fine grain to be produced during the dynamic recrystallization process; thus, most welds formed at 14 mm/min have a smaller grain size.

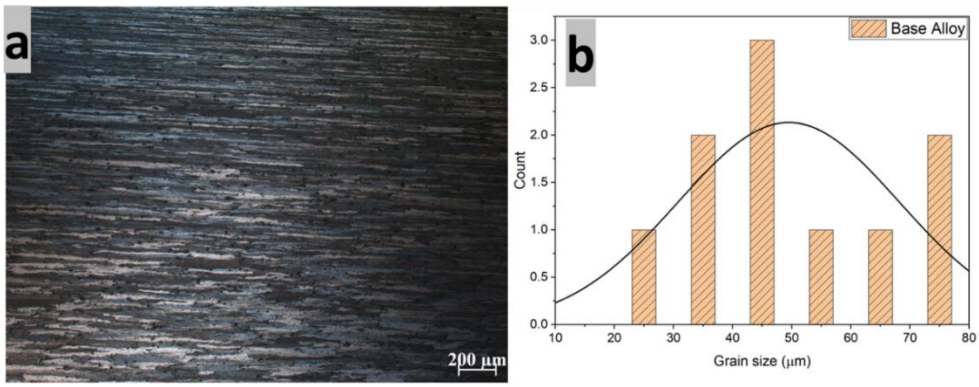

Fig. 4 AA1050 rolled base alloy (a) Optical microstructure image, (b) Histogram of the grain size distribution

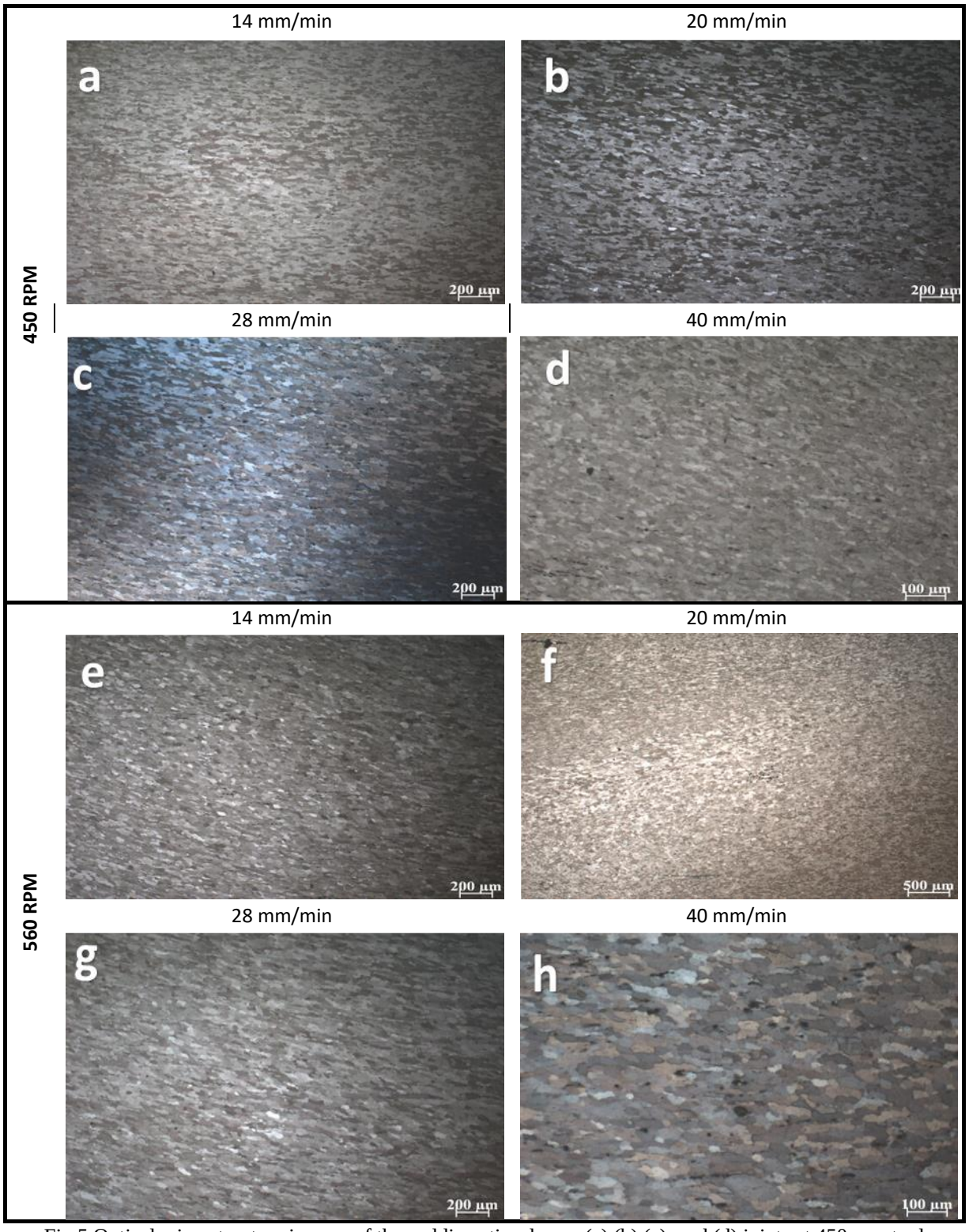

Fig.5 Optical microstructure images of the welding stirred zone (a),(b),(c), and (d) joints at 450 rpm tool rotational speed and 14, 20, 28, and 40 mm/min welding speeds; (e),(f),(g) and (h) joints at 560 rpm tool rotational speed and 14, 20, 28 and 40 mm/min welding speeds.

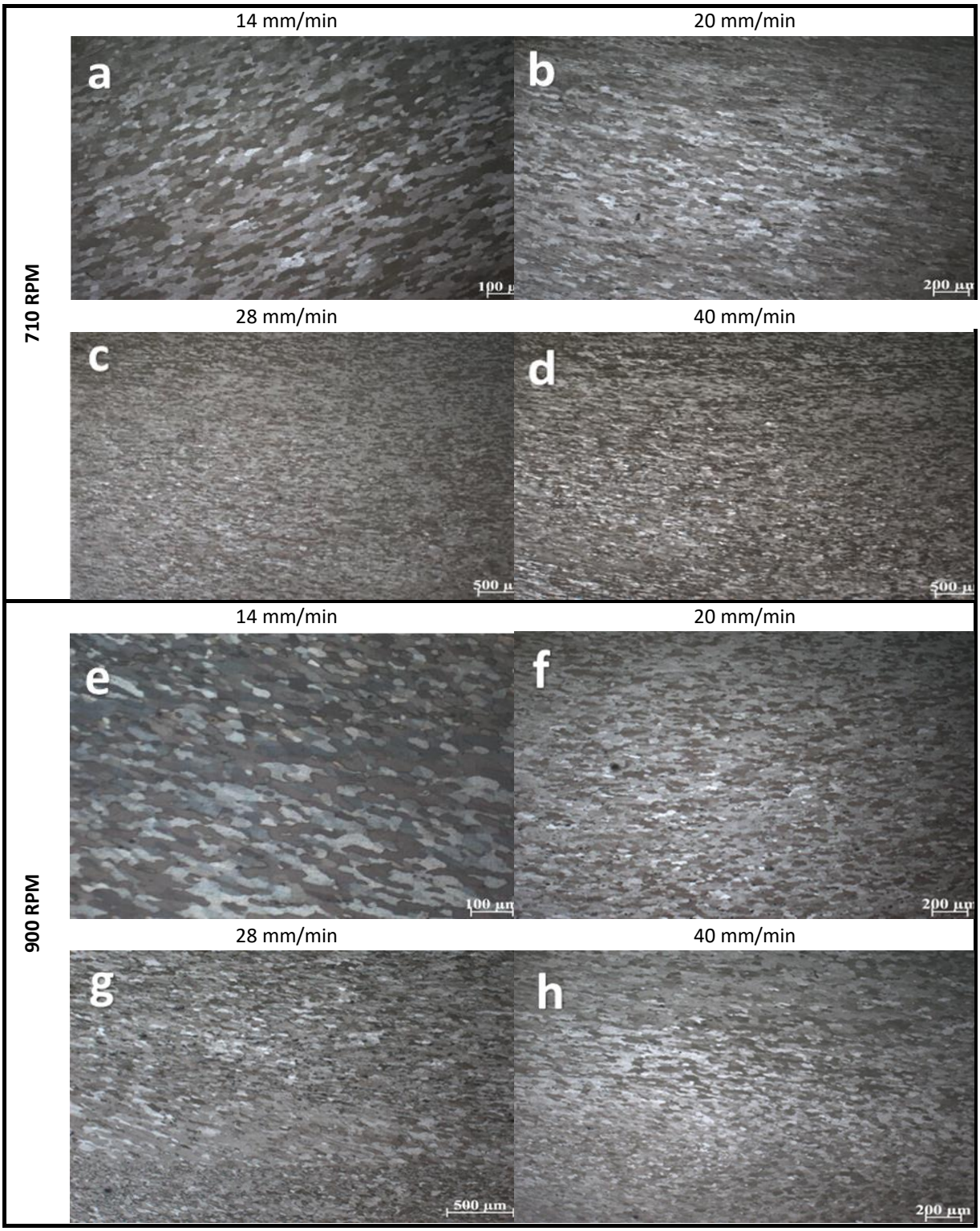

Fig.6 Optical microstructure images of the welding stirred zone (a),(b),(c) and (d) joints at 710 rpm tool rotational speed and 14, 20, 28 and 40 mm/min welding speeds; (e),(f),(g) and (h) joints at 900 rpm tool rotational speed and 14, 20, 28 and 40 mm/min welding speeds .

Grain size aspect ratio of the stirred welding zone and base AA1050 alloy

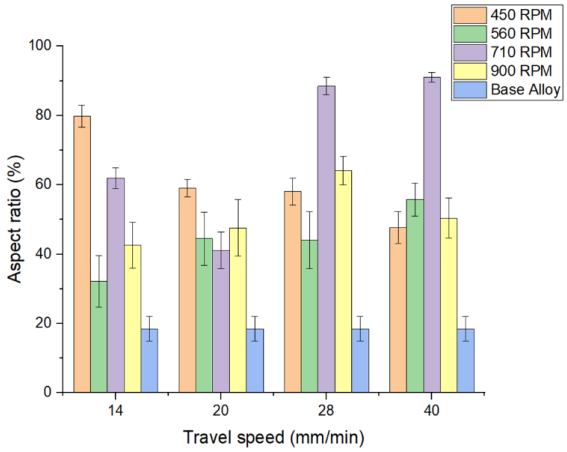

Fig. 8 Effect of the welding speed on the AVG grain size

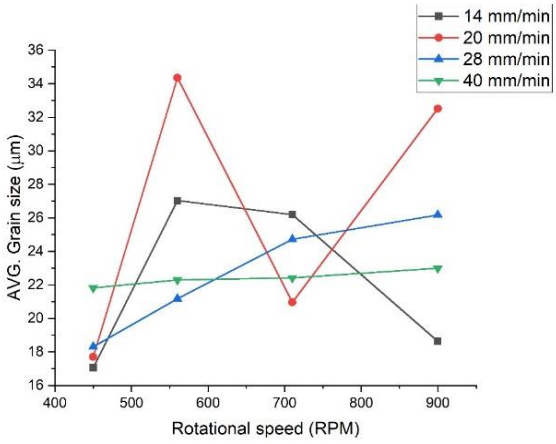

Fig. 9 Effect of the tool rotation speed on the stirred zone grain size

3.2 Heat Generation Prediction Model

The heat prediction model of the friction stir welding process has been developed in order to help optimize welding parameters. According to the experimental data, ANSYS software simulates the welding process. The model considers the process of friction stir welding, including the frictional melting of the aluminum substrates, the plasticity of the aluminum substrate due to high temperatures, the strain of the Al substrate, the strain hardening of the substrate, and the heat generation. The model has been validated through experimental tests. The friction stir welding process is characterized by two main phases: the heating phase and the melting phase. During the heating phase, a high-temperature gradient is created, the molten zone of the material is formed, and a crater is created due to material removal from the surface.

During the melting phase, a zone with a low-temperature gradient is created between the hot spots in contact with the tool and the rest of the material at lower temperatures than the hot spots. The empirical equation is used to predict the maximum temperature developed during the welding process. Thus equation (1) is obtained from the regression analysis of the real experimental measurement. Fig.10 shows the fitting curve of the empirical prediction equation for maximum temperature.

The model's parameters include the material properties, the tool geometry, and the stirring parameters. It is used for predicting heat generation during the friction stir welding process. Figure 11 shows the simulated temperature gradient of the welding process.

$$T_{max} = 94.7 \times e^{(-r/0.033)} + 466.6 \qquad (1)$$

where the r = (welding speed /tool rotation speed).

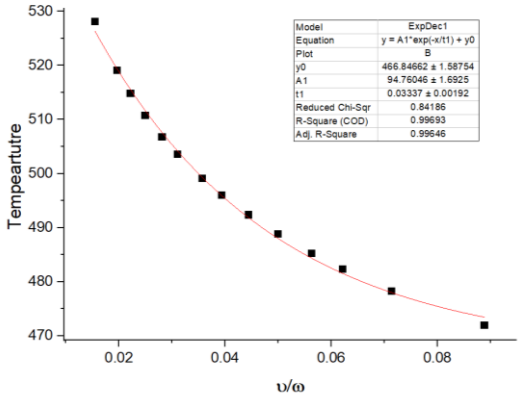

Fig. 10 Fitted curve plot

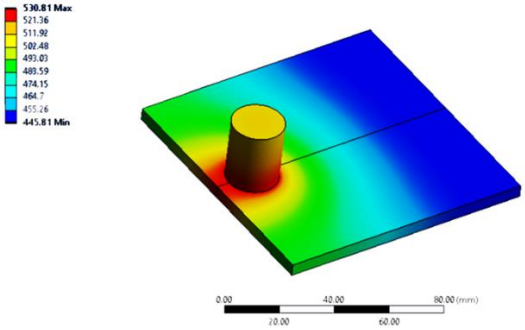

Fig.11 The simulation of the predicted heat generation in the welded joint.

3.3 Effect of The Maximum Temperature of the Microstructure Grain Refinement

The microstructure refinement of weld metal is one of the most important aspects in the fabrication and quality control of friction stir welded joints. The grain

refinement process in the weld metal is due to the undercooling produced by the heat generated during the friction stir welding process. The undercooling causes the grain growth rate to increase because of the low thermal activation barrier. The grain refinement mechanism is also determined by the amount of heat generated during the friction stir welding process. Grain refinement is closely related to heat generation during the friction stir welding process. The results show that the grain size increases with the heat generated during friction stir welding. The increase in the heat generated during the friction stir welding process results in the formation of grain boundaries, which provide new pathways for the diffusion of solute atoms; the results are consistent with [34, 35]. These new atoms are consumed at the grain boundaries. This process reduces the grain size and also reduces the grain boundary thickness, thus increasing the mobility of the atoms in the bulk material [36]. Figure 12 shows the relationship between the friction stir welding parameters and the corresponding average grain size resultant in the stirred zone. The results reveal that the AA1050 does not need extra heat to execute the welding process; thus, 450 rpm is enough to accomplish the process with low heat and excellent grain refinement.

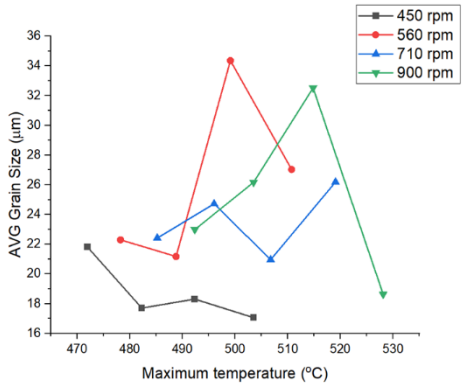

Fig.12 correlation between the maximum generated temperature and corresponding grain size at different welding speeds 14, 20, 28, and 40 mm/min

3.4 Microhardness Behavior

Microhardness testing has shown the base metal to be 31.5 HV0.1. From the microhardness profile, as shown in Fig. 13, it is clear that the FSW process reduced the hardness in the processed zone. Due to the high temperatures (about 546 degrees Celsius), the FSW in the stirred zone is expected to have the lowest hardness of the weld zone, as shown in the thermal image Fig. 14. This is because the precipitation phase dissolves in this zone due to the high temperatures. The border between the HAZ and the TMAZ, also known as the low-hardness zone, was the location of the observed decrease in microhardness (LHZ). The lowest observed hardness reduction was at 710 rpm tool rotation speed and 40 mm/min welding speed. Otherwise, all readings are very close. A second inference that can be made is that the microhardness varies very little at different distances away from the weld face.

In most cases, the portion of the material located closer to the shoulder of the tool has more severe reductions in its microhardness. The most significant takeaway from this study is that the microhardness and position of the LHZ are highly dependent on the particular parameters of the welding process used, as shown in Fig 15. The amount of heat introduced during the welding process is the most important variable, as this produces the strengthening phase and brings grain growth to an average. The mean hardness value of the stirred zone was observed to be lower than the base metal by 24.5 %; thus, the maximum and minimum reductions in the microhardness value through the tested samples were 20.7 % and 33.5 %. Table 3 illustrate the relationship between microhardness values and associated processing parameters.

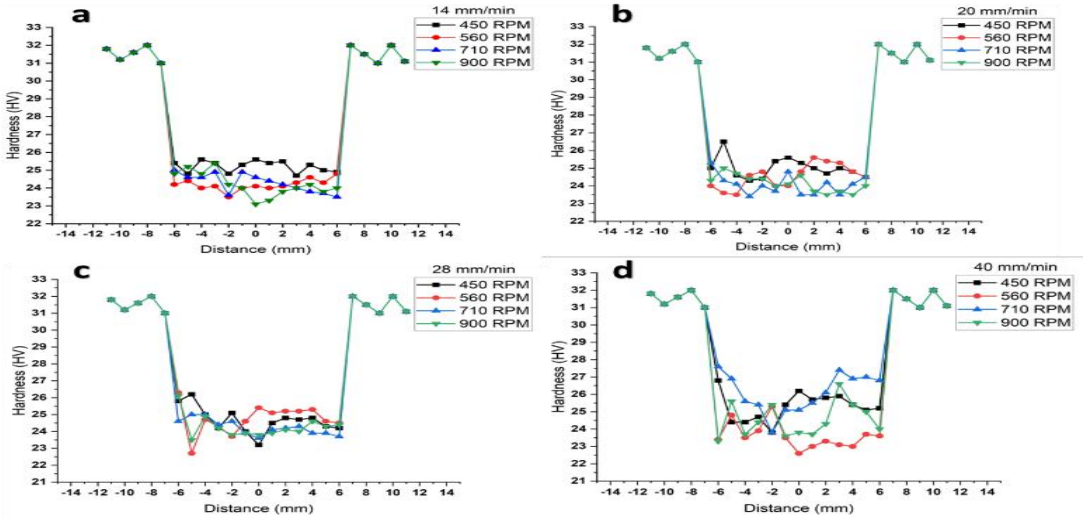

Fig.13 Microhardness profile of the base metal and welding stirred zone (a) travel speed of 14 mm/min, (b) travel speed of 20 mm/min, (c) travel speed of 28 mm/min, (d) travel speed of 40 mm/min.

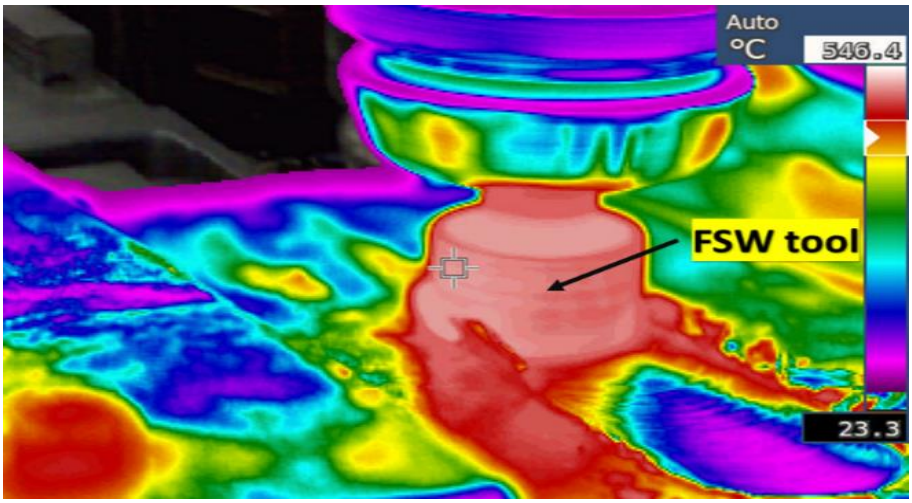

Fg.14 Thermal image of the FSW process

Table 3: Microhardness values with their corresponding processing parameters

Too rotation speed (RPM)	Tool travel speed (mm/min)	AVG. Microhardness (H.V.)	Standard Deviation (StD)	Microhardness reduction (%)
450	14	25.2	0.32	25
	20	25	0.6	26
	28	24.7	0.77	27.6
	40	25.3	0.82	24.5
560	14	24.2	0.32	30.2
	20	24.5	0.68	28.4
	28	24.7	0.88	27.3
	40	23.6	0.74	33.5
710	14	24.3	0.53	29.7
	20	24.1	0.57	30.9
	28	24.2	0.46	29.9
	40	26.1	1.11	20.7
900	14	24.2	0.68	30.2
	20	24.1	0.47	30.5
	28	24.3	0.66	29.8
	40	24.5	0.99	28.5
Base alloy	-----	31.5	0.28	00

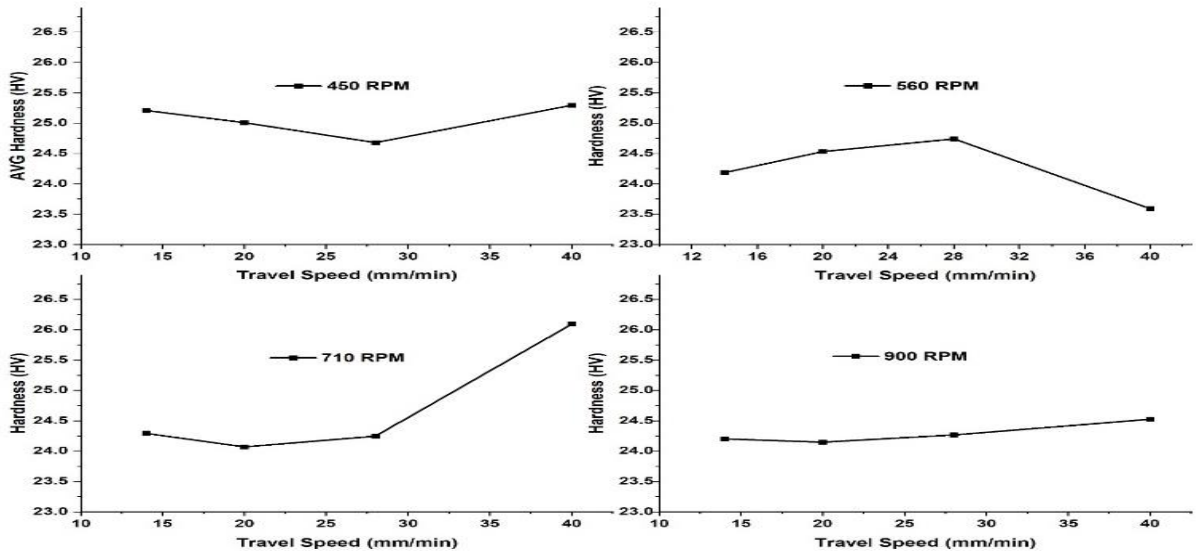

Fig. 15 The AVG.microhardness value of the tested samples at a different tool rotation speed.

4. Conclusion

The AA1050 aluminum alloy sheets have been welded using the friction stir welding technique in the current investigation. The influence of the processing parameters on the microstructure and microhardness behavior has been studied. As the grain size of the agitated zone increases with increasing speed. Heat input increases with rotation speed Recrystallization increases grain growth, heat input, and rotation speed due to the ω/v ratio. Because dynamic recrystallization produces finer grains at lower traverse speeds, most welds with 14 mm/min traverse speed have smaller grain sizes. The welding process zone's hardness was reduced by the FSW method due to the high heat generated between the shoulder and base metal. The grain refinement during the DRX process also affects the microhardness. No significant change in hardness properties was observed in the present study, indicating that the metal transfer rate does not influence the values obtained for the FSW welds. Moreover, the results of the present investigation indicate that the reduction in the porosity level in the weld created by a higher value for the metal transfer rate can significantly decrease the hardness of the FSW weld. Predicting the maximum heat generation during the FSW process helps further to predict models for mechanical properties and grain size.

Conflicts of Interest

"There are no conflicts to declare."

References

[1] A. Heidarzadeh, S. Mironov, R. Kaibyshev, G. Çam, A. Simar, A. Gerlich, F. Khodabakhshi, A. Mostafaei, D.P. Field, J.D. Robson, A. Deschamps, P.J. Withers, Friction stir welding/processing of metals and alloys: A comprehensive review on microstructural evolution, Progress in Materials Science, 117 (2021) 100752.

[2] W. He, J. Liu, W. Hu, G. Wang, W. Chen, Controlling residual stress and distortion of friction stir welding joint by external stationary shoulder, 38 (2019) 662-671.

[3] E. Moustafa, Effect of Multi-Pass Friction Stir Processing on Mechanical Properties for AA2024/Al2O3 Nanocomposites, in: Materials, 2017.

[4] W.S. AbuShanab, E.B. Moustafa, Detection of Friction Stir Welding Defects of AA1060 Aluminum Alloy Using Specific Damping Capacity, in: Materials, 2018.

[5] N.Z. Khan, D. Bajaj, A.N. Siddiquee, Z.A. Khan, M.H. Abidi, U. Umer, H. Alkhalefah, Investigation on Effect of Strain Rate and Heat Generation on Traverse Force in FSW of Dissimilar Aerospace Grade Aluminium Alloys, in: Materials, 2019.

[6] E.B. Moustafa, A. Melaibari, G. Alsoruji, A.M. Khalil, A.O. Mosleh, Tribological and mechanical characteristics of AA5083 alloy reinforced by hybridising heavy ceramic particles Ta2C & V.C. with light GNP and Al2O3 nanoparticles, Ceramics International, 48 (2022) 4710-4721.

[7] E.B. Moustafa, Hybridization effect of B.N. and Al2O3 nanoparticles on the physical, wear, and electrical properties of aluminum AA1060 nanocomposites, Applied Physics A, 127 (2021) 724.

[8] S.S. Nayak, R.P. Mahto, S.K. Pal, P. Srirangam, Microstructure and Texture in Welding: A Case Study on Friction Stir Welding, in: J.P. Davim (Ed.) Welding Technology, Springer International Publishing, Cham, 2021, pp. 193-228.

[9] K.S. Arora, S. Pandey, M. Schaper, R. Kumar, Effect of process parameters on friction stir welding of aluminum alloy 2219-T87, The International Journal of Advanced Manufacturing Technology, 50 (2010) 941-952.

[10] S.A. Khodir, T. Shibayanagi, Friction stir welding of dissimilar AA2024 and AA7075 aluminum alloys, Materials Science and Engineering: B, 148 (2008) 82-87.

[11] A.H. Feng, D.L. Chen, Z.Y. Ma, Microstructure and Cyclic Deformation Behavior of a Friction-Stir-Welded 7075 Al Alloy, Metallurgical and Materials Transactions A, 41 (2010) 957-971.

[12] C.B. Fuller, M.W. Mahoney, M. Calabrese, L. Micona, Evolution of microstructure and mechanical properties in naturally aged 7050 and 7075 Al friction stir welds, Materials Science and Engineering: A, 527 (2010) 2233-2240.

[13] C.A.W. Olea, L. Roldo, J.F. dos Santos, T.R. Strohaecker, A sub-structural analysis of friction stir welded joints in an AA6056 Al-alloy in T4 and T6 temper conditions, Materials Science and Engineering: A, 454-455 (2007) 52-62.

[14] E.B. Moustafa, A.H. Elsheikh, M.A. Taha, The effect of TaC and NbC hybrid and mono-nanoparticles on AA2024 nanocomposites: Microstructure, strengthening, and artificial aging, 11 (2022) 2513-2525.

[15] J.m.V. Leon.J., Investigation of mechanical properties of aluminium 6061 alloy friction stir welding International Journal of Students' Research in Technology & Management, 2 (2014) 140-144.

[16] C. Rajendran, K. Srinivasan, V. Balasubramanian, H. Balaji, P. Selvaraj, Feasibility study of FSW, LBW and TIG joining process to fabricate light combat aircraft structure, International Journal of Lightweight Materials and Manufacture, 4 (2021) 480-490.

[17] M. Peel, A. Steuwer, M. Preuss, P.J. Withers, Microstructure, mechanical properties and

residual stresses as a function of welding speed in aluminium AA5083 friction stir welds, Acta Materialia, 51 (2003) 4791-4801.
[18] B.K.B. Nadikudi, Parametric optimization of friction stir welding process parameters of dissimilar welded joints using grey relational analysis and desirability function approach, World Journal of Engineering, ahead-of-print (2022).
[19] T.A. Shehabeldeen, Y. Yin, X. Ji, X. Shen, Z. Zhang, J. Zhou, Investigation of the microstructure, mechanical properties and fracture mechanisms of dissimilar friction stir welded aluminium/titanium joints, Journal of Materials Research and Technology, 11 (2021) 507-518.
[20] B. Li, Y. Shen, L. Luo, W. Hu, Effects of processing variables and heat treatments on Al/Ti-6Al-4V interface microstructure of bimetal clad-plate fabricated via a novel route employing friction stir lap welding, Journal of Alloys and Compounds, 658 (2016) 904-913.
[21] E.B. Moustafa, W.S. AbuShanab, E. Ghandourah, M.A. Taha, Microstructural, mechanical and thermal properties evaluation of AA6061/Al2O3-BN hybrid and mono nanocomposite surface, Journal of Materials Research and Technology, 9 (2020) 15486-15495.
[22] B. Kuang, Y. Shen, W. Chen, X. Yao, H. Xu, J. Gao, J. Zhang, The dissimilar friction stir lap welding of 1A99 Al to pure Cu using Zn as filler metal with "pinless" tool configuration, Materials & Design, 68 (2015) 54-62.
[23] V. Balasubramanian, Relationship between base metal properties and friction stir welding process parameters, Materials Science and Engineering: A, 480 (2008) 397-403.
[24] J. Das, P.S. Robi, P.K. Sahu, Influence of process parameters on mechanical and microstructural properties of friction stir welded AA5052, Advances in Materials and Processing Technologies, (2022) 1-17.
[25] V. Mishin, I. Shishov, A. Kalinenko, I. Vysotskii, I. Zuiko, S. Malopheyev, S. Mironov, R. Kaibyshev, Numerical Simulation of the Thermo-Mechanical Behavior of 6061 Aluminum Alloy during Friction-Stir Welding, in: Journal of Manufacturing and Materials Processing, 2022.
[26] P.A. Colegrove, H.R. Shercliff, R. Zettler, Model for predicting heat generation and temperature in friction stir welding from the material properties, Science and Technology of Welding and Joining, 12 (2007) 284-297.
[27] M. Mehta, A. Arora, A. De, T. DebRoy, Tool Geometry for Friction Stir Welding—Optimum Shoulder Diameter, Metallurgical and Materials Transactions A, 42 (2011) 2716-2722.
[28] M. Reza-E-Rabby, W. Tang, A. Reynolds, Effect of Tool Pin Features and Geometries on Quality of Weld During Friction Stir Welding, in: R. Mishra, M.W. Mahoney, Y. Sato, Y. Hovanski, R. Verma (Eds.) Friction Stir Welding and Processing VII, Springer International Publishing, Cham, 2016, pp. 163-171.
[29] E.B. Moustafa, Dynamic Characteristics Study for Surface Composite of AMMNCs Matrix Fabricated by Friction Stir Process, Materials, 11 (2018).
[30] W.S. AbuShanab, E.B. Moustafa, Effects of friction stir processing parameters on the wear resistance and mechanical properties of fabricated metal matrix nanocomposites (MMNCs) surface, Journal of Materials Research and Technology, 9 (2020) 7460-7471.
[31] B. Chaudhary, V. Patel, P.L. Ramkumar, J. Vora, Temperature Distribution During Friction Stir Welding of AA2014 Aluminum Alloy: Experimental and Statistical Analysis, Transactions of the Indian Institute of Metals, 72 (2019) 969-981.
[32] E.B. Moustafa, W.S. Abushanab, A. Melaibari, O. Yakovtseva, A.O. Mosleh, The Effectiveness of Incorporating Hybrid Reinforcement Nanoparticles in the Enhancement of the Tribological Behavior of Aluminum Metal Matrix Composites, JOM, 73 (2021) 4338-4348.
[33] K.V. Jata, S.L. Semiatin, Continuous dynamic recrystallization during friction stir welding of high strength aluminum alloys, Scripta Materialia, 43 (2000) 743-749.
[34] M.M. Ahmed, S. Ataya, M.M. Seleman, T. Allam, N.A. Alsaleh, E. Ahmed, Grain Structure, Crystallographic Texture, and Hardening Behavior of Dissimilar Friction Stir Welded AA5083-O and AA5754-H14, in: Metals, 2021.
[35] X. Qin, Y. Xu, Y. Sun, H. Fujii, Z. Zhu, C.H. Shek, Effect of process parameters on microstructure and mechanical properties of friction stir welded CoCrFeNi high entropy alloy, Materials Science and Engineering: A, 782 (2020) 139277.
[36] R.M. German, Chapter Seven - Thermodynamic and Kinetic Treatments, in: R.M. German (Ed.) Sintering: from Empirical Observations to Scientific Principles, Butterworth-Heinemann, Boston, 2014, pp. 183-226.